

# Synthesis and Characterization of Colloidal Model Particles Made from Organoalkoxysilanes

A. van Blaaderen and A. Vrij

Van't Hoff Laboratory, University of Utrecht, Padualaan 8, 3584 CH  
Utrecht, The Netherlands

*Monodisperse colloidal silica spheres were prepared by hydrolysis and condensation of tetraethoxysilane (TES) in a mixture of water, ammonia, and a lower alcohol. These silica spheres were coated with the coupling agent 3-aminopropyltriethoxysilane (APS) in the reaction medium. A new colloidal model system that was prepared consisted of a stable dispersion of monodisperse, hybrid, organic-inorganic "silica" spheres. Particles were characterized by  $^{13}\text{C}$  and  $^{29}\text{Si}$  NMR spectroscopy, elemental analysis, transmission electron microscopy, and static and dynamic light scattering. The particles made from TES alone (with radii between 15 and 100 nm) consisted of partially condensed siloxane structures, which were approximately the same for all particle sizes. Thus, the siloxane structure did not reflect differences in the particle shape and surface roughness. The percentage of silicon atoms not bonded to four other silicons, but bonded to one hydroxyl or ethoxy group, was close to 30%. A few percent of silicons had only two siloxane bonds, and at least a few percent of the ethoxy groups were present in the core of the particles, having never been hydrolyzed. Thus, hydrolysis probably is the rate-determining step in base-catalyzed particle growth. Further, the particle radius could be altered only by addition of  $\text{LiNO}_3$ , if the salt was added to the reaction mixture at the start of the reaction. Thus, the ionic strength provides a new parameter to study the reaction mechanism. Its influence confirms that the particles form through a controlled aggregation process of homogeneously precipitating nuclei early in the reaction. Monodispersity and a smooth particle surface are achieved through subsequent monomer addition. The new parti-*

0065-2393/94/0234-0083\$09.62/0

© 1994 American Chemical Society

*cles prepared from a mixture of APS and TES contained, on a silicon basis, as much as 26% APS distributed through the particle interior.*

**M**ONODISPERSE COLLOIDAL SILICA SPHERES with various surface coatings are of considerable interest to many fields, such as ceramics, colloids, catalysis, chromatography, and glass preparation. We are interested in these particles for their use as a model colloid. Previous work (1–9) has shown that by using scattering techniques, much insight can be gained in the interparticle structure and dynamics of concentrated dispersions. To avoid, for example, multiple scattering, it is important to determine and change the chemical microstructure of the (single) colloidal particles. The surface coating determines the solvents in which the colloids can be dispersed and the kind of interactions between colloidal spheres. An understanding of the mechanisms responsible for particle formation and the coating of its surface is very important to tailor the scattering properties and particle interactions.

Through the hydrolysis and condensation of tetraalkoxysilanes in mixtures of ammonia, water, and alcohols, (uncoated) silica particles are easily prepared by using a method developed by Stöber et al. (1). The experimental procedure is very simple, but the mechanisms responsible for the formation and growth of the charge-stabilized silica spheres are not. A generally accepted scheme has not yet been presented. A tentative mechanism for the nucleation and growth is described in this chapter, based on an analysis of the final particle morphology and chemical microstructure. A description is also given of the use of the silane coupling agent 3-aminopropyltriethoxysilane (APS) to prepare model colloids.

APS is known for its stability in basic solutions (10). The amine functionality facilitates the coupling of other desired molecules to a particle. For these reasons, this alkoxide was chosen to coat the surface of the Stöber silica spheres. A simple procedure was followed, first described by Philipse and Vrij (4), who used other coupling agents. Badley et al. (11) also described the coupling of APS and other organosilanes to silica.

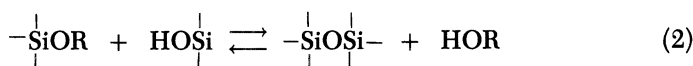
APS and tetraethoxysilane (TES) were also used in the synthesis of a new kind of monodisperse colloidal system. Spherical particles were made by starting from a mixture of the organoalkoxysilanes TES and APS. This procedure will probably be applicable to other mixtures of organoalkoxysilanes as well.

The microstructure and particle morphology (size, shape, and surface roughness) of the colloids were studied with  $^{13}\text{C}$  and  $^{29}\text{Si}$  NMR spectroscopy, elemental analysis, transmission electron microscopy, and static and dynamic light scattering.

To facilitate the interpretation and to place the proposed mechanism into perspective, a literature survey is presented. Relevant details concerning the base-catalyzed chemistry and characterization of alkoxysilanes by NMR spectroscopy and some of the proposed particle formation and growth theories are given.

### *Theory and Earlier Work*

**Reactions and Chemical Mechanisms.** Alkoxysilanes in a mixture of water, ammonia, and a lower alcohol may undergo many different reactions. Reactions between the different silane intermediates can be represented as follows:



Here R and R' stand for a hydrogen atom or an alkoxy group (methoxy, ethoxy, or propoxy). The other atoms bonded to silicon that are not depicted can either be carbon (in the organoalkoxides), or oxygen (belonging to a silanol and alkoxy group or a siloxane bond). The breaking of a C-Si bond and direct ester exchange between the alkoxides are not considered possible (12). We will discuss only base-catalyzed reactions.

The reactions in equation 1 constitute ester exchange, hydrolysis, and their reversals. In the base-catalyzed case these reactions proceed through a nucleophilic attack on the silicon atom, resulting in a pentacoordinate transition state (12-15).

We first consider the hydrolysis and the influence on its rate by some reaction conditions. OH<sup>-</sup> is acting as the nucleophile; an increase in the concentration of this catalyst will increase the reaction rate. OH<sup>-</sup> is produced by reaction of NH<sub>3</sub> with H<sub>2</sub>O. The rate increases almost linearly with [NH<sub>3</sub>] (16). As expected, the hydrolysis appears to be first order in TES (16, 17). The dependence of the rate constant on [H<sub>2</sub>O] is even higher, according to Harris et al. (18), than the dependence on [NH<sub>3</sub>]: [H<sub>2</sub>O]<sup>1.5</sup>. The effect on the reaction rate of changing the solvent alcohol is quite complex, and further experimental work and a theoretical explanation are needed (15-18).

The influence of a substituent on the silicon atom can be derived from its ability to withdraw electrons or its steric hindrance to an attacking nucleophile. For these reasons, the lower alkoxides are hydrolyzed faster than the higher and branched alcohol derivatives. Hydrolysis of a given alkoxide proceeds in successive steps. Because the alkoxy group is less

electron-withdrawing and more bulky than a hydroxy group, each successive loss of an alkoxy group is accompanied by an increase in the rate of loss of the next.

The base-catalyzed condensation reactions in equation 2 also take place through a base-catalyzed nucleophilic attack on silicon resulting in a pentavalent transition complex (12, 15, 19, 20). The influence of  $[\text{H}_2\text{O}]$  and  $[\text{NH}_3]$  on the reaction rate and the type of alcohol used is almost the same as for the hydrolysis (12, 18).

An important question to be explained by the chemical mechanism is why base catalysis often leads to condensed structures. In 1950, Aelion et al. (13) pointed out that the condensation reaction in base-catalyzed systems was faster than with acid catalysis and that the microstructure of the final product was different. Many of these facts are due to the opposite effects of, for example, substituents, on silicon on the stabilization of the transition state in base- and acid-catalyzed reactions (15). For the base-catalyzed condensation reaction to take place, a silicon atom has to be attacked by a deprotonated silanol oxygen: the nucleophile. The acidity of the silanol proton increases as the basicity of the other groups bonded to the silicon decreases. This feature implies that polysilicic acid is a stronger acid than  $\text{Si}(\text{OH})_4$  (20). Therefore, monomers react preferentially with higher polymerized species.

Under certain conditions (for instance, high  $[\text{TES}]$  or low water concentrations), the reaction between not fully hydrolyzed species must also be considered. In this case the condensation and hydrolysis reactions can occur in one step: After attack of a silanolate ion, the transition state can subsequently lose an alkoxy group. Alkoxy groups that end up on a highly condensed unit are then much more difficult to hydrolyze because of steric constraints.

The replacement of an alkoxy group causes an inductive effect. Binding of an organofunctional group through a C–Si bond decreases both the hydrolysis rate and the condensation rate through the same mechanism. The less electronegative carbon makes a nucleophilic attack on silicon more difficult.

This reasoning also applies to APS: Compared to TES, base-catalyzed hydrolysis and condensation are slower for APS. However, in some respects this molecule does not behave like other silane coupling agents. Solutions of APS in water are quite stable at basic pH values, whereas solutions of other coupling agents rapidly form insoluble precipitates under the same conditions (21). This difference in behavior is explained by Plueddemann (21) by assuming that the hydrolyzed APS forms a six- or five-membered chelate ring. The six-membered ring is thought to form by binding of the amine with a silanolate ion and the pentacoordinate complex by binding between nitrogen and silicon. No direct evidence has been found for one of these structures. Most likely, one of them exists, because

compounds with one CH<sub>2</sub> group more or less in the aliphatic chain do not display the increased stability of APS and rapidly form precipitates in water. Moreover, these precipitates remained insoluble after they were acidified, a result indicating that the insolubility is not caused by the amine portion (15).

**Nucleation and Growth: Results from the Literature.** Before discussing different mechanisms of nucleation and growth that have appeared in the literature, we first present some general observations about the hundreds of silica sols that have been described (1, 2, 4–7, 16–18, 22–28) and synthesized according to Stöber.

Most of the work was done with the alkoxide TES and the alcohol ethanol as solvent. Lowering the temperature always results in larger particles. Sometimes the radius can become 4 times larger by lowering the temperature 30 °C (26). In the range of TES concentrations in which particles seem to be stable, larger particles generally tend to be more monodisperse. Standard deviations in particle size of only 2% have been observed.

Mostly, particles are larger when synthesized from higher concentrations of TES, although the increase in radius is quite small, and sometimes the opposite trend is described (2). After the reactants are mixed, the turbidity of the solution suddenly rises after a certain induction time and then slowly increases to its final value. The induction time is closely related to the total time of the particle growth. If the particles reach their final radius in a short time, the induction period is also short.

Increasing [H<sub>2</sub>O] and [NH<sub>3</sub>] results in faster reactions and initially, at low concentrations, in larger radii. However, both H<sub>2</sub>O and NH<sub>3</sub> show a concentration for which a maximum radius is achieved. Increasing the concentration any further still gives shorter reaction times, but the radius decreases. Near these maxima the sols sometimes flocculate and are not so monodisperse. This instability is also found in the limits of high TES or high NH<sub>3</sub> concentrations. Under some conditions, particles with a grainy surface are observed.

Increasing the length of the solvent *n*-alcohol results in larger particles (1, 16–18, 22). Densities of the resulting homogeneous particles were reported in the range 1.9–2.1 g/mL, and the refractive index was found close to 1.45 (2, 3, 26).

Matsoukas and Gulari (17) convincingly showed that the particle mass grows exponentially with the same time constant that describes the first-order hydrolysis of TES. They used the plasma lines in a Raman spectroscopy experiment to observe not only the intensities of the Si–O–Et and Et–OH bands, but at the same time used the light scattering of the particles to follow their growth. The induction period found in the scattering experiments was not found for the hydrolysis reaction.

Subsequently, Matsoukas and Gulari (22) worked out a model describing the nucleation and growth in more detail. In a purely kinetic theory, they formulated a monomer addition model in the presence of a rate-determining first-order initiation step and investigated the effect of different particle growth models upon the final particle size and polydispersity. In their model the dynamic competition between nucleation and growth is controlled by the hydrolysis that releases the active monomer. This monomer is produced in a slow hydrolysis reaction that inhibits nucleation and, therefore, promotes growth of large particles.

In the model, two limits are considered: a reaction-limited growth, which is characterized by a strong size dependence of the growth rate, and diffusion-limited growth, with much weaker size dependence. These limits refer only to the bonding between a particle and a monomer; the overall rate is still governed by the hydrolysis.

The actual rate equations are based on a succession of irreversible steps. Hydrolysis is modeled as first order in TES and produces the active monomer. These monomers can react with another monomer forming the (second-order) nucleation step, or can react with an already higher condensed species. All the subsequent addition steps are considered elementary and are described with different rate constants  $k_i$  (with  $i$  the number of monomers that formed the particle). Generally,  $k_i$  depends on the radius ( $R$ ) of the particle. The limit that  $k_i$  is independent of the particle size was assumed to represent a reaction-limited growth (the correct dependence is  $k_i \sim R$ ), and  $k_i$  proportional to the particle volume ( $R^3$ ) was assumed to represent diffusion-limited growth (the correct dependence is  $k_i \sim R^2$ ). Under these assumptions, Matsoukas and Gulari (22) derived for the final particle radius ( $R$ ) the following expressions:

$$R \sim (k_p c / k_h)^{1/9} \quad \text{diffusion-limited growth} \quad (3)$$

$$R \sim (k_p c / k_h)^{1/6} \quad \text{reaction-limited growth} \quad (4)$$

where  $k_p$  and  $k_h$  are the polymerization and hydrolysis rate constants, respectively, and  $c$  is the starting TES concentration.

Using the correct dependencies of the rate constants  $k_i$  on the particle size, they also obtained expressions relating the final polydispersity to the final mean particle radius  $\langle R \rangle$ :

$$\sigma^2 \sim \langle R \rangle^{-3} \quad \text{diffusion-limited growth} \quad (5)$$

$$\sigma^2 \sim \langle R \rangle^{-2} \quad \text{reaction-limited growth} \quad (6)$$

In the experimental part the relations between equations 3 and 6 were tested; the data were best described with a reaction-limited growth (in the presence of a rate-limiting hydrolysis of the monomers). The increase in

particle size with increasing ammonia concentration was rationalized by stating that, although this effect resulted in an increase in  $k_h$ ,  $k_p$  would have to increase even further.

Bogush and co-workers (24, 26, 27) investigated the Stöber synthesis using electron microscopy, conductivity measurements, and the (small) change in reaction medium volume. They concluded that all the TES hydrolyzes completely in the first few minutes and that the Stöber silica particles are formed through a size-dependent, controlled, coagulative nucleation and growth mechanism. They argued that nucleation from the extremely supersaturated solutions continued almost to the point at which the particles reached their final size. In the beginning of the reaction, small unstable particles aggregate until a critical size is reached at which the probability of two particles of equal size sticking together becomes negligible. Homogeneous nucleation still continues, and the freshly formed small particles are taken up by the large stable particles that now remain constant in number. Classical nucleation expressions were used to estimate nucleation rates per unit volume (29, 30). Their proposed size-dependent nucleation–aggregation mechanism is analogous to a similar model developed to explain the emulsion polymerization of styrene (31).

Philipse (5) also assumed that fast hydrolysis created an active monomer bulk. He studied the growth of silica nuclei, already synthesized, after extra addition of different amounts of TES with static light scattering. To explain his growth curves (radius versus time), he used a diffusion-controlled particle growth in a finite bulk of monomers or subparticles. The model contained equations from classical flocculation theories. It takes into account the exhaustion of the monomer bulk and the retarding influence of an (unscreened) electrostatic repulsion between growing spheres and monomers.

Harris and co-workers (16, 18) concluded that the Stöber system obeyed La Mer's homogeneous nucleation and growth model (32). In this scheme the slow hydrolysis of TES builds up the critical concentration of silicic acid required to form nuclei. The short nucleation phase then lowers the concentration of silicic acid below its critical value, followed by growth of monodisperse silica particles. Monodispersity is always achieved if the nucleation phase is short enough, whether the growth process is diffusion- or reaction-controlled (33). They found that under conditions where the amount of silicic acid remained relatively high (that is, a few times the equilibrium value) during an important part of the reaction, the resulting sol was polydisperse.

Schaefer and Keefer (14, 19, 34, 35) used a model developed by Eden to describe the growth of cell colonies to explain their X-ray scattering experiments. They used this simple model of nucleation and chemical limited growth to mimic the growth of silica structures in TES solutions (1

M) with a relatively low water concentration (1–4 M) and with very little catalyst, 0.01 M  $\text{NH}_3$ .

In their version of the Eden model, one starts with a seed, that is, one site on a two-dimensional lattice, and randomly chooses and occupies one of the four neighboring sites. The next growth site is picked from the resulting six neighboring sites, etc. This method results in spherical particles with uniform interiors and smooth surfaces relative to their radii.

The fact that the interior becomes uniform seems an artifact, because growth is even allowed in free places inside a particle. The formation of such regions in three-dimensional growth is very unlikely, so allowing this kind of growth inside a particle in the two-dimensional model makes comparison with three-dimensional studies more realistic.

The effects on the particle shape of particle formation from partially hydrolyzed monomers were also investigated. By choosing certain mixtures of monomers, Schaefer and Keefer generated all kinds of particle morphologies, from porous clusters to surface and mass fractals.

**Silicon Environments and Solid-State NMR Spectroscopy.** Magic-angle spinning (MAS) and high-power proton decoupling (HPD) make it possible in solid-state NMR spectroscopy to obtain high-resolution  $^{13}\text{C}$  and  $^{29}\text{Si}$  spectra. These techniques average the chemical-shift anisotropy and dipolar interactions that otherwise would cause very broad lines. In a liquid this averaging is accomplished by the rapid thermal motions of the molecules in the magnetic field.

The NMR solid-state technique of cross-polarization (CP) consists of a transfer of magnetization from  $^1\text{H}$  nuclei to  $^{13}\text{C}$  or  $^{29}\text{Si}$  nuclei through dipolar interactions. In this way, selective detection of only those  $^{13}\text{C}$  and  $^{29}\text{Si}$  nuclei that are near protons becomes possible. For silica consisting mainly of  $\text{SiO}_2$ , this technique entails a selective detection of only those nuclei close to the surface where OH groups and other proton-containing species are present. In addition to this selectivity, CP enhances the sensitivity of the NMR experiment and shortens the necessary delay between acquisitions of successive transitions to a few seconds. For the  $^{29}\text{Si}$  nucleus that can have spin-lattice relaxation times ( $T_1$ ) of minutes, this enhanced sensitivity can be important.

Through siloxane bonds, a silicon atom can be bonded to a maximum of four other silicon nuclei. If a  $^{29}\text{Si}$  nucleus is bonded to four other silicon atoms, the chemical shift of this so-called  $\text{Q}^4$  species lies around  $-110$  ppm. The  $\text{Q}^4$  representation comes from the old silicon-chemistry (12); the Q stands for quaternary (that is, having the possibility of forming four siloxane bonds). The number 4 gives the actual number of siloxane bonds in which the nucleus is participating (Figure 1). For every siloxane bond less, a shift of about 10 ppm occurs. Therefore,  $\text{Q}^2$  has a chemical shift around  $-110 + 2 \times 10 = -90$  ppm.



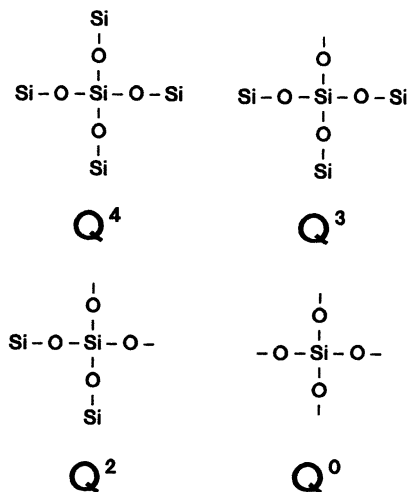


Figure 1. Silicon environments. Groups not depicted are alkoxy or silanol.

The exchange of one Si-O bond with a Si-C bond makes a significant difference in chemical shift. For APS this exchange results in a shift +40 ppm. The organosilane is now designated T<sup>0</sup> to T<sup>3</sup> (T from ternary).

Clearly these features make silicon NMR spectroscopy a valuable technique in examining the microstructure of silica and its derivatives (36–40). However, almost no difference in chemical shift is seen between a silicon atom that has an alkoxy and one that has a hydroxy group bonded to it. Carbon solid-state NMR spectroscopy is useful to determine the presence of alkoxy groups and to detect the carbon atoms of a coupling agent if present.

## Experimental Details

**Materials and Particle Preparation.** Methanol (Baker), ethanol (Merck), and 1-propanol (Baker) were of analytic reagent quality. Absolute technical grade ethanol (Nedalco) was used only for the large-scale (9 L) synthesis of A1. Solvents, tetraethoxysilane (Fluka, purum grade) and  $\gamma$ -aminopropyltriethoxysilane (Janssen) were freshly distilled before each synthesis. Ammonium hydroxide (Merck, 25%) was of analytical reagent quality and contained 14.0 mol/L NH<sub>3</sub> as indicated by titration. The silicas Ludox AS40 and Compol were kindly provided by DuPont and Fujimi.

Alcosols, silica particles dispersed in the reaction medium, were synthesized at 20 °C according to the method of Stöber et al. (1) and the detailed description given by Van Helden et al. (2). Glassware was cleaned with 6% hydrogen fluoride and rinsed with deionized water and absolute ethanol. Ammonium hydroxide, ethanol, and, if necessary, deionized water were mixed in a reaction vessel and placed in a constant-temperature bath. After allowing the temperature to come to equilibrium, the TES was added under vigorous stirring. After a few minutes the

reaction was continued using a slow stirring speed. The total amount of alcosol varied between 0.4 and 9 L. Concentrations of reactants used are given in Table I; in their calculation, volume contraction was assumed to be absent.

Table I. Reactant Concentrations

System	[TES] (M)	[APS] (M)	[H <sub>2</sub> O] (M)	[NH <sub>3</sub> ] (M)	Solvent
A1	0.155		0.855	0.318	ethanol
A1APS <sup>a</sup>		0.477	0.855	0.318	ethanol
A2	0.0119		5.51	0.682	ethanol
A3	0.17		1.65	0.68	ethanol
A4	0.167		1.58	0.512	ethanol
A5 <sup>b</sup>	0.159		3.01	1.12	ethanol
A5APS <sup>a</sup>		0.205	3.01	1.12	ethanol
A6	0.160		2.65	0.986	ethanol
A7 <sup>c</sup>	0.160		2.65	0.986	eth-LiNO <sub>3</sub>
A8 <sup>c</sup>	0.160		2.65	0.986	eth-LiNO <sub>3</sub>
Mix1	0.0809	0.0774	2.34	0.870	ethanol
M1	0.161		2.50	0.928	methanol
P1	0.178		1.03	0.383	propanol

<sup>a</sup>Alcosol taken as reaction medium for the coating reaction.

<sup>b</sup>Reaction temperature was 25 °C; all other reactions were at 20 °C.

<sup>c</sup>[LiNO<sub>3</sub>] = 1.0 mM. For A8 the LiNO<sub>3</sub> was added before TES, and A7 was added 15 min after TES.

For the coating reactions with APS (Table I), a procedure similar to that described by Philippe and Vrij (4) was applied. Philippe and Vrij used the coupling agent 3-methacryloxypropyltrimethoxysilane to coat colloidal silica. Because an alcosol was used, the actual concentrations of water as listed in Table I have to be corrected for the (not exactly known) amount consumed in the hydrolysis-condensation reactions. After addition of the APS to 400 mL of alcosol, the solution was stirred slowly for an hour. After 2 h of refluxing, 250 mL was distilled slowly for an hour. The remaining unreacted APS was removed in four centrifugation redispersion steps. The ultracentrifuge used was from Beckmann (L5-50B), and the sediment was redispersed each time in absolute ethanol.

Silica spheres with APS distributed in the particle interior were prepared by adding APS (Table I) first to the reaction mixture. Subsequently an equal volume of TES was added within 1 min. Free APS was again separated from the particles by centrifugation and redispersing in ethanol. Particle densities were measured by drying, under dry nitrogen for 24 h at 100 °C, a known volume of a concentrated dispersion in absolute ethanol and weighing the residue.

Alcosols are referred to in this chapter as Ax, with x being a numeral. The A is replaced by a P or a M if the alcohol used was not ethanol but 1-propanol or methanol, respectively (Table I). Coated particles are designated AxAPS and AxS; the last code stands for a coating with stearyl alcohol according to the procedure developed by Van Helden et al. (2). *Mix* denotes particles prepared from a mixture of the alkoxides TES and APS. Some of these systems have been used in earlier work with different names, so some translation is necessary. A3S is designated in several investigations as SJ9 (9). SM2, known here as A1, is described by Penders and Vrij (41). The Ludox and Compol systems are described elsewhere by Duits et al. (42).

**Light Scattering.** Light-scattering measurements were made at  $25 \pm 0.1$  °C on dust-free, very dilute dispersions in ethanol. The dispersions were made by adding one drop of alcohol to 25 mL of ethanol followed by filtration through Millipore filters (the pore was typically several particle diameters). Cuvets with a diameter of 2 cm were cleaned by continuously rinsing with freshly distilled acetone.

Static light scattering (SLS) was performed with a Fica-50 photometer using vertically polarized light ( $\lambda = 436$  and  $546$  nm). A correction was made for scattering of the solvent. The Rayleigh-Gans-Debye approximation could be used, and the particles were assumed to be spherical and to have a homogeneous refractive index. Under these assumptions, the particle radius ( $R_0$ ) was obtained from a fit of the calculated form factor to the scattered intensity as a function of the scattering angle  $\theta$  ( $20^\circ \leq \theta \leq 150^\circ$ ). Intensities at low angles are sensitive to dust or clustered particles (2); no irregularities were found, a result indicating monodisperse, nonclustered sols.

Dynamic light scattering (DLS) results were obtained with an argon ion laser (Spectra Physics Series 2000) operating at 488.0 and 514.5 nm. Autocorrelation functions were measured with a Malvern Multibit K7025 128-point correlator. Diffusion coefficients were obtained from a second-order cumulant fit (43, 44) by using autocorrelation functions obtained from six scattering angles between  $35^\circ$  and  $145^\circ$ . From the diffusion coefficient, a hydrodynamic radius  $R_h$  was calculated by using the Stokes-Einstein relation. Except for dispersion A1, the normalized second cumulant yielded values smaller than  $\sim 0.05$ ; the value for A1 was around 0.12. More information can be found elsewhere about the procedures and equipment of SLS (3, 6) and DLS (45, 46).

**Elemental Analysis.** Elemental analysis was carried out by Elemental Microanalysis Limited (Devon, U.K.). Prior to shipping, the samples were dried for 24 h at 100 °C under nitrogen; before the measurements were made, they were dried again for 3 h under the same conditions.

**Electron Microscopy.** Transmission electron micrographs were made by dipping copper 400-mesh carrier grids in a dilute dispersion. The grids were covered with carbon-coated Formvar films, and the photographs were made of particles on the film. Philips EM301 and Philips CM10 transmission electron microscopes were used, with the magnification calibrated with a diffraction grating.

Some of the particles were studied after supercritical point drying. The particles were dispersed in acetone by several centrifugation steps ( $45,000 \times g$ ). In a critical point dryer (Balzers Union, CPD 020), the carbon-coated grids and the dispersion in acetone were placed. Under pressure, the acetone was exchanged against liquid  $\text{CO}_2$ ; after increasing the temperature and passing the critical point, the particles adsorbed on the film were supercritically dried.

Particle radii of 500–2000 particles were measured with an interactive image analysis system (IBAS). From these data, a number-averaged particle radius  $\langle R \rangle$  and a standard deviation  $\sigma$  defined by:

$$\sigma = \left[ \frac{\langle R^2 \rangle - \langle R \rangle^2}{\langle R \rangle^2} \right]^{1/2} \quad (7)$$

were determined.

**NMR Spectroscopy.** High-resolution solid-state NMR spectra were measured at room temperature on a Bruker AM 500 spectrometer (silicon frequency 99.4 MHz and carbon, 125.7 MHz) equipped with a Bruker solid-state accessory. Spectra were obtained with a broad-band probehead with a 7-mm double air-bearing magic-angle spinning (MAS) assembly. Spinning speeds around 4000 Hz were employed. The 90° pulse lengths for the nuclei  $^{13}\text{C}$ ,  $^{29}\text{Si}$ , and  $^1\text{H}$  were around 5.5  $\mu\text{s}$ . The spectra that were obtained with cross-polarization had contact times between 0.5 and 2 ms for carbon and between 0.5 and 6 ms for silicon; pulse sequences were repeated after 4s. The number of accumulated free induction decays (FIDs) per spectrum ranged between 200 and 4000, depending on the system being investigated.

Quantitative silicon spectra were obtained by using 90°  $^{29}\text{Si}$  pulses; it was not necessary to use high-power proton decoupling. Even at the high magnetic field used, the relatively small chemical-shift anisotropy and dipolar coupling with protons could be removed completely by MAS alone. Because, for some samples, the  $\text{Q}^4$  silicon atoms had spin-lattice relaxation times of about 90 s, the time delay between 90° pulses was chosen as long as 400 s. Typically, 200 FIDs were accumulated. Deconvolution of the spectra was performed by manually adjusting the height, width, and frequency of the Gaussian line shapes to obtain the best visual fit.

The samples used for NMR spectroscopy were freeze-dried to prevent any reaction during the drying process. Adamantane and the trimethylsilyl ester of double four-ring octameric silicate,  $\text{Q}^8\text{M}^8$  were used to optimize experimental parameters and as external secondary (relative to TMS) chemical-shift references for  $^{13}\text{C}$  and  $^{29}\text{Si}$ , respectively. Both the  $T_1$  measurements and a discussion on the use of  $^{29}\text{Si}$  NMR spectroscopy for quantitative measurements will be described elsewhere (47).

## Results and Discussion

In this section, experimental results obtained with several different experimental techniques and measured on several different colloidal silica dispersions are described and discussed. The ultimate goal of the investigations is the ability to synthesize stable, monodisperse colloidal model spheres from organoalkoxysilanes with different chemical compositions and surface properties (47–52).

The first step was the synthesis of several colloidal systems with different radii from TES alone (A1–A6), and comparison of these particles with commercially available systems that were prepared in a different way, such as Ludox and Compol (20). The stabilities of the sol and the radii were probed with static and dynamic light scattering (SLS and DLS, respectively) because these techniques are sensitive to particle clustering. The polydispersity in the particle size, particle shape, and surface roughness (all these particle properties are further referred to as the particle morphology) were investigated with transmission electron microscopy (TEM). The chemical microstructure of the particles or, more precisely, the siloxane structure of the final particles and the presence of alkoxy groups were investigated with solid-state silicon and carbon NMR,

combined with elemental analysis. To obtain more information on the particle formation mechanism, two colloidal systems were made by using a different alcohol as solvent (M1 and P1), and two systems were made after addition of  $\text{LiNO}_3$  to change the ionic strength (A7 and A8).

The second step consisted of the coating of several "Stöber" silica particles with APS and the synthesis of a new kind of particles from a mixture of APS and TES. The colloidal dispersions obtained were also characterized by the techniques just mentioned.

**Particle Morphology (SLS, DLS, and TEM).** In this section the results of the "Stöber" silica particles are presented, followed by the Ludox and Compol particles, and finally the particles made with APS. Then, the results relevant to a tentative formation and growth model are discussed.

All the synthesized alcosols except M1 remained stable for months, as indicated by light scattering. M1 flocculated 2 weeks after the synthesis but did not show any sign of instability directly after the reaction.

The general trends on the dependence of the final particle radius on the concentrations of  $\text{NH}_3$  and water, on the alcohol used as solvent, and on the temperature can be found in Tables I and II. Increasing the concentrations of  $\text{NH}_3$  and water results in larger radii (compare for example, A1, A4, and A5). This effect is no longer true for very high concentrations of water (A2). Increasing the temperature decreased the radius (compare A5 and A6). Going from methanol to propanol increases the radius (compare M1, A1, and P1).

An interesting new result is the strong dependence of the radius on the ionic strength if this is increased *before* the addition of TES (A6, A7, and A8, Tables I and II).  $\text{LiNO}_3$  was chosen to change the ionic strength because it dissociates completely in this concentration range (53). The flocculation concentration of the sol A6 was 5 mM of  $\text{LiNO}_3$ .

The radii  $R_o$  and  $R_h$  as obtained with SLS and DLS, respectively, show reasonable-to-good agreement (Table II). The small differences and the small corrections that can be made if the polydispersity is taken into account are discussed in more detail elsewhere (9, 49). The differences between the light-scattering radii and the radii as obtained with TEM are not negligible and cannot be explained by the differences in the averages that are determined with the different experimental techniques (2, 9). As was suggested by Van Helden et al. (2) we attribute these differences to radiation damage that causes the particles to shrink somewhat. (The drying process does not influence the radius determined with TEM, because no differences were observed between normally and supercritically dried samples.)

Despite the fact that the absolute radii are probably too small, the polydispersities determined with TEM are correct. As is known from the

Table II. Radii According to Transmission Electron Microscopy and Static and Dynamic Light Scattering

System	TEM <sup>a</sup> (nm)	SLS (nm)	DLS (nm)
A1	9.01 (20%)		9 ± 2
A1APS	9.15 (20%)		14 ± 3
A2	50.2 (150%)		
A3S	30.9 (13%)	39.6 ± 0.5	38.5 ± 0.5
A4	31.2 (13%)	40.2 ± 0.5	36.6 ± 1.6
A5	62.4 (11%)	71.5 ± 0.4	72.1 ± 1.2
A5APS	66.1 (11%)	73.6 ± 0.5	80 ± 3
A6	89.4 (6%)	107.2 ± 0.3	108.1 ± 0.7
A7	93.2 (8%)	109.4 ± 0.4	
A8	154.3 (8%)	179.3 ± 0.4	
Mix1	92.2 (11%)	128 ± 2	118 ± 3
M1	18.2 (16%)	26.1 ± 0.9	30 ± 2
P1	24.2 (12%)	33.1 ± 0.5	35.1 ± 1.3
Ludox	11.1 (20%)	17.5 ± 0.3	20.8 ± 0.5
Compol	50.5 (16%)		

<sup>a</sup>The number in parentheses is the relative standard deviation.

literature (1, 2, 26), the polydispersities decrease as the mean radius increases. The only exception is A2, but this system was made from a very low concentration of TES (Table I).

The appearance of "Stöber" silica particles may depend strongly on the conditions under which they were made (2, 4–7, 24–27). Particles have been described as being irregular, roughly spherical, spherical, and large, flocculated, and fused structures (28). All the different types of morphology can be seen in the electron micrographs of the various alcosols shown in Figure 2, except for the flocculated structures. The irregularly shaped particles were not deformed in any way by capillary forces (20), because some samples (A1 and A4) were supercritically dried, a condition that eliminates the effects of the surface tension. Probably because of the high speed of centrifugation needed to settle these small particles, a fraction of them appeared to be clustered after redispersing in acetone. However, the amount of separately laying particles (Figure 2a) was sufficient to clearly demonstrate that both the form and radius were the same when compared with a sample of A1 that was not supercritically dried. Figure 2e shows another highly magnified supercritically dried particle (A4). The particle shown in Figure 2e had the characteristics of particles that are smaller than ~70-nm radius and are synthesized from concentrations of TES around 0.17 M. These smaller "Stöber" particles are only roughly spherical and possess a grainy irregular surface (Figure 2d). However, the particles A2 prepared from a low concentration of TES and a high concentration of

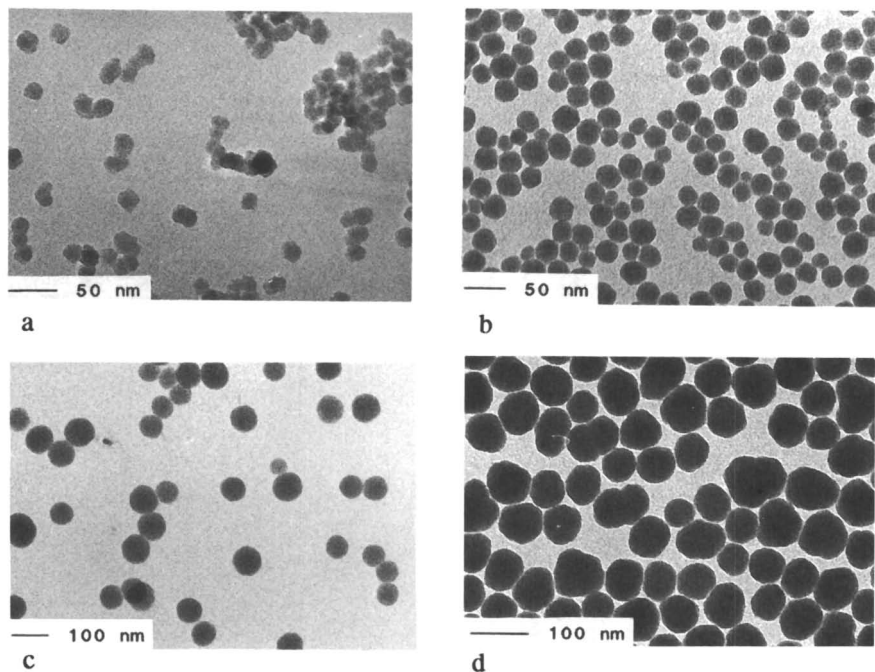


**Figure 2.** Transmission electron micrographs. Part a: A1,  $\langle R \rangle = 9.01$  nm (20%), supercritically dried. Part b: Ludox,  $\langle R \rangle = 11.1$  nm (20%). Part c: A2,  $\langle R \rangle = 50.2$  nm (150%). Part d: A3S,  $\langle R \rangle = 30.9$  nm (13%). Continued on next page.

water (Table I) are small, but almost perfect spheres with very smooth surfaces. Only the polydispersity is very high.

In Figure 2g a typical larger Stöber particle (A6) is shown. These particles are smooth and almost perfect spheres. Comparing the shape of the Ludox particles (Figure 2b) and the Compol particles (Figure 2f) with the Stöber particles of about the same size (Figure 2a and 2d) shows only small differences. The particles not synthesized from TES are slightly more spherical, and the surfaces are somewhat less rough.

The micrographs of the APS-coated particles were not different from the uncoated spheres and are therefore not shown. In Figure 2h the particles Mix1 are shown. Considering the amount of APS that is part of these particles, it is amazing how spherical and monodisperse these particles are. Clearly, all the organic groups (disrupting the siloxane structure) inside the particles do not influence the final particle shape. When compared with A6, they appear only slightly rougher. The difference in density between these two systems is considerable and is visible in the micrographs. The density of Mix1 is 1.51 g/mL, and that of A6 is 2.08 g/mL (50).

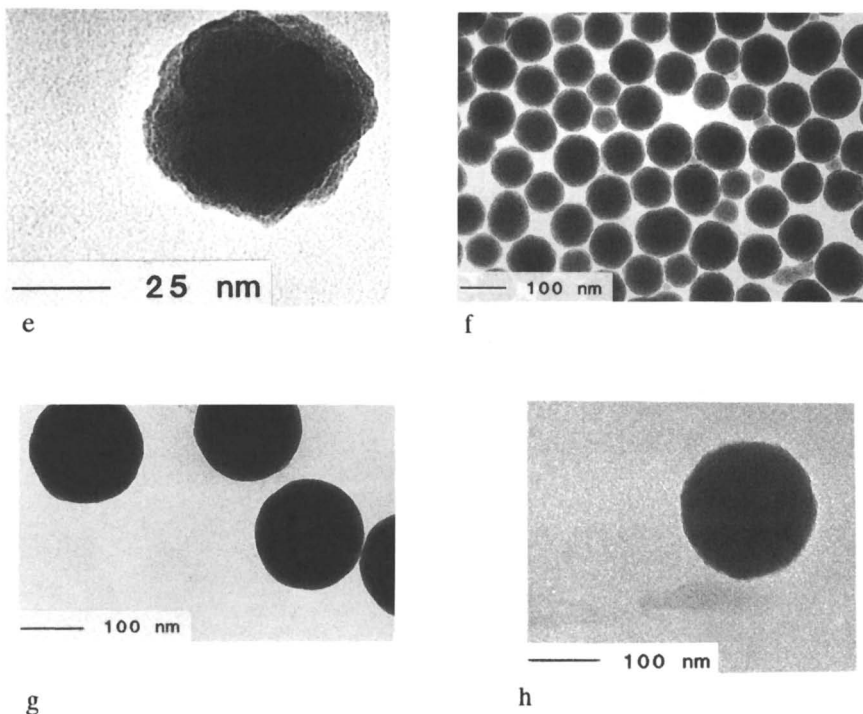


Figure 2.—Continued. Transmission electron micrographs. Part g: A6,  $\langle R \rangle = 89.4$  nm (7%). Part h: Mix 1,  $\langle R \rangle = 92.2$  nm (11%).

**Particle Microstructure (NMR Spectroscopy and Elemental Analysis).** The  $^{29}\text{Si}$  CP NMR spectra were much easier to obtain than the direct excitation spectra, because of the long spin-lattice relaxation time of the silicon nuclei. Nevertheless, direct excitation was used to obtain the quantitative results of the siloxane structure, because not all  $\text{Q}^4$  nuclei were detected with CP (Figure 3 and Table III) (47).

Surprisingly, all the quantitative spectra of the alcosol particles looked similar. As is also demonstrated in Table III, the siloxane structure of all the Stöber silica spheres is more or less constant and independent of the particle size and thus the reaction conditions. Even the coated stearylsilica particle A3S is no exception, despite the 3 h at 200 °C necessary for the coating. Thus, the differences mentioned in the previous section in the particle morphology are not correlated with the siloxane structure.

The colloidal particles Ludox and Compol consist of a more condensed silica structure (Table III). As mentioned, CP detects only those nuclei that have dipolar interactions with protons. Because of the condensed structure, a significant number of  $\text{Q}^4$  silicon nuclei is too far away from protons and is not detected in a CP experiment (contrary to  $\text{Q}^4$  nuclei in the alcosol



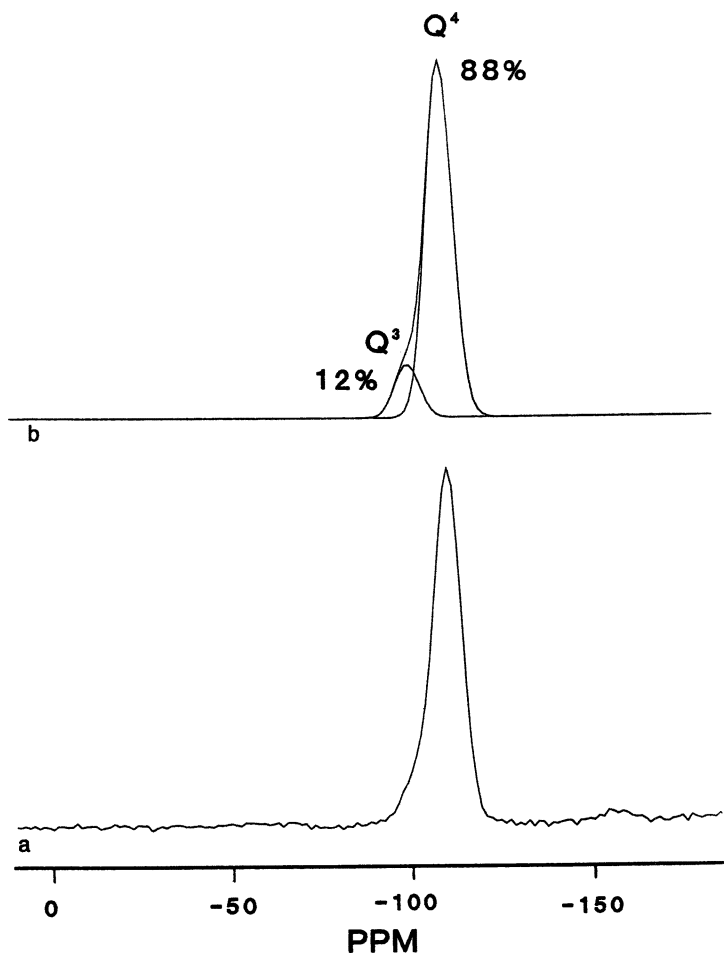


Figure 3.  $^{29}\text{Si}$  NMR spectra of Compol. Part a: Direct polarization MAS, 300 accumulations, and repetition time of 400 s. Part b: Deconvoluted spectrum using Gaussian line shape. Continued on next page.

particles). An example of this effect can be seen in Figure 3a and 3c of the Compol particles. The spectrum in Figure 3a was obtained by using direct polarization through  $90^\circ$  pulses, MAS, and repetition times of 400 s. CP-MAS was used for Figure 3c. The CP spectrum, Figure 3c, contains more  $\text{Q}^3$  signal than  $\text{Q}^4$ , whereas the quantitative spectrum, Figure 3a, shows no detectable amount of  $\text{Q}^2$ , and only 12% of  $\text{Q}^3$  against 88%  $\text{Q}^4$ .

The Ludox silica structure can be calculated to be more or less fully condensed. The surface and volume of a Ludox sphere are calculated from the radius (e.g., 11 nm, Table II). Assuming 4.5 OH groups per square nanometer (20), the expected number of silanol groups as a percentage of

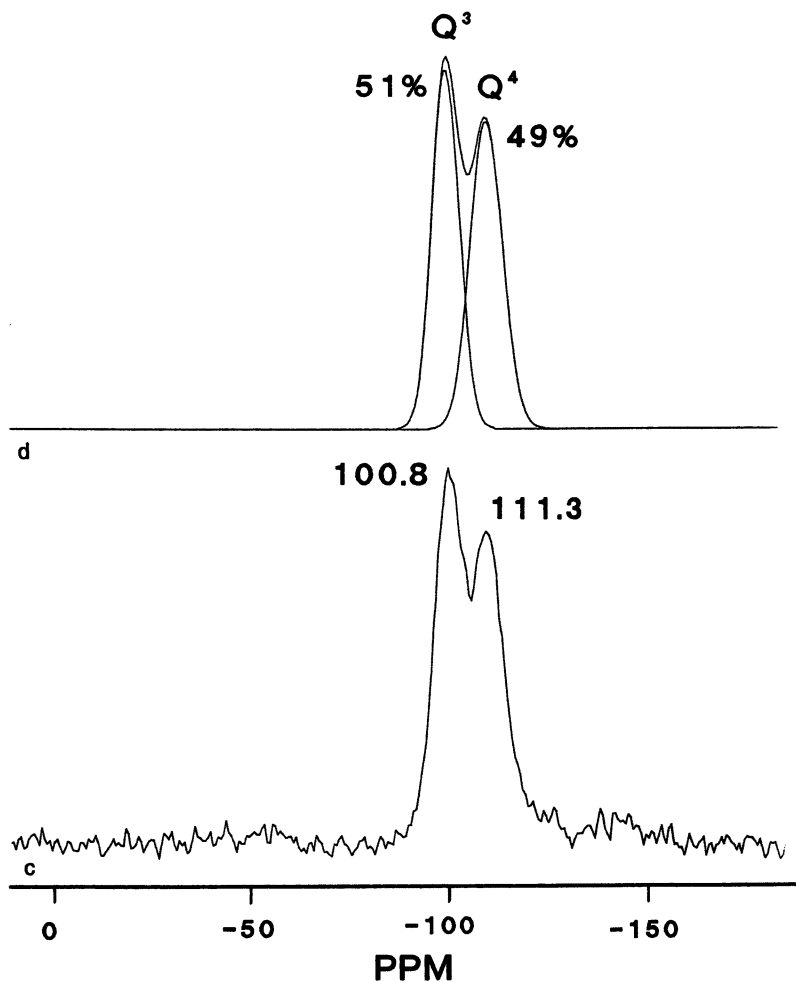


Figure 3.—Continued.  $^{29}\text{Si}$  NMR spectra of Compol. Part c: CP-MAS, 2000 accumulations, repetition time of 4 s, and contact time of 4 ms. Part d: Deconvoluted spectrum using Gaussian line shape.

the number of silicon atoms per particle can be determined. The number of silicon atoms in the particle can be obtained from the density [2.2 g/mL (20)] and the molecular weight, which is, taking 15%  $\text{Q}^3$  into account, 61.43 g/mol. These calculations result in a percentage of silanol groups of 5.7%. This amount is small compared to the experimental number of 15% as obtained by NMR spectroscopy. It may be clear, however, that some surface roughness, as was observed by TEM, will increase the surface area. Because the siloxane structure of the Compol particles is close to that of

**Table III. Relative Intensities of the Different Types of Silicon Environments**

<i>System</i>	$Q^4$	$Q^3$	$Q^2$	$T^3$	$T^2$
A1 <sup>a</sup>	73 <sup>b</sup>	26	1.7		
A1APS	67	21	—	7.2	4.4
A2	69	32	—		
A3S	65	31	4.1		
A5 <sup>a</sup>	64	31	5.5		
A5APS	65	30	4.0	—	—
A6	66	30	4.2		
Mix1	40	31	3.8	19	7.2
M1	64	30	6.5		
P1	66	28	5.6		
Ludox	85	15	—		
Compol	88	12	—		

NOTE: Data are reported as percentages. Blank cells indicate that the nuclei could not be present in the sample. Dashes indicate that the numbers were too small to be determined.

<sup>a</sup>The same reaction procedures as for the coating were followed, except for the addition of APS.

<sup>b</sup>Estimated errors for  $Q^4$  and  $Q^3$  were  $\pm 2\%$ ; for the other species,  $\pm 1\%$ .

Ludox, and the radius is about 5 times larger, it is also clear that even the Compol particles are not fully condensed  $\text{SiO}_2$  with only silanol groups at the particle surface.

$^{13}\text{C}$  CP-MAS NMR spectroscopy showed the presence of ethoxy groups for all the alcosols prepared in ethanol, in accordance with elemental analysis (Table IV). The carbon next to oxygen was found close to 60 ppm, and the methyl group was at around 17 ppm (Figure 4a). The stearyl-coated A3S was no exception: an important part of the carbon signals originated from ethoxy groups. The carbon content of the larger particles, A5 and A6, is even higher than that of the particles A1. This result seems to indicate that for the larger particles most of the ethoxy groups are trapped inside the particles. This hypothesis is corroborated by a washing procedure of A6 (Table IV), which did not remove much of the carbon content. For the particles with a (much) higher surface area, the effect of washing with water (P1 in Table IV) or the refluxing of the particles A1 was visible in a significant change in carbon content. The almost complete removal of the carbon content for P1 after washing seems to suggest that the particles are microporous.

The chemical shifts of a carbon next to an OH group or next to O-Si are very close together. If only one O-C carbon is found, it is difficult to distinguish between ethoxy groups chemically bound and ethanol molecules bonded through hydrogen bonds with silanol groups. Another

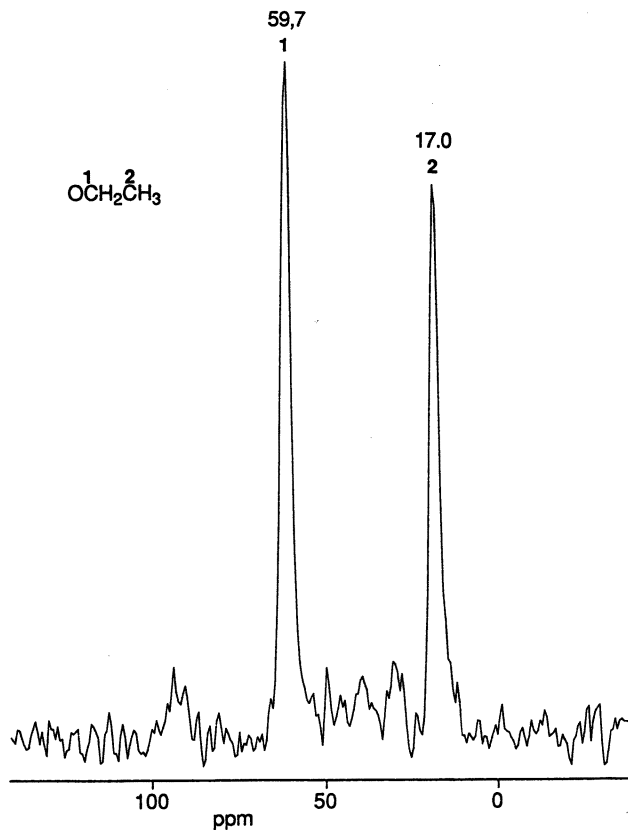


Figure 4.  $^{13}\text{C}$  CP-MAS NMR spectra of alkoxy groups in silica; contact time of 2 ms. Part a: A1, 1000 accumulations.

possibility for the origin of the ethoxy signals in the  $^{13}\text{C}$  alcosol spectra is reesterification of hydrolyzed silanol groups.

To resolve the questions raised in the previous paragraph, particles were synthesized in methanol and 1-propanol. Complete hydrolysis and reesterification in these solvents would result in the appearance of only methoxy and propoxy groups. The  $^{13}\text{C}$  CP-MAS spectra of A1, P1, and M1 are shown in Figure 4. Ethoxy groups can still be seen in both particles prepared in methanol and propanol. No reesterification of ethoxy groups is possible in these solvents; thus the detected groups must never have left the TES molecule. Although care must be taken in using CP spectra quantitatively, it is probably safe to conclude from Figure 4 and Table IV that between 10% and 30% of the detected carbon in the elemental analysis belongs to ethoxy groups from TES. The amount of silicon atoms with ethoxy groups bonded to them that have never left the original TES

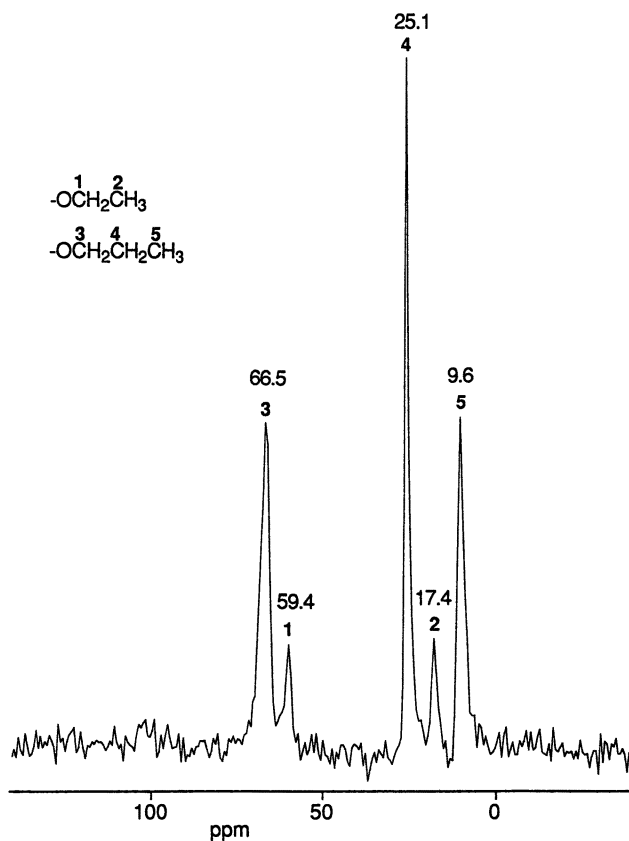


Figure 4.—Continued. Part b: P1, 500 accumulations. Continued on next page.

molecule is at least a few percent, whereas some reesterification or ester exchange seems to take place as well.

If the carbon and proton weight percentages are subtracted from 1 g of particles (Table IV), the remainder of the weight can be equalized to  $n\text{SiO}_x$ , where  $x$  can be determined from the relative intensities of Q species as determined by NMR spectroscopy (Table III). The carbon content can be used to calculate the number of ethoxy groups. The number of silicon atoms with bonded ethoxy groups ranges from almost zero (for the particles A2 made in a relatively high concentration of water) to 14% for sample A5.

For the sample A3S, the amount of silicon was determined: 39.0% (elemental analysis described in reference 4). Subtracting C and H and using the siloxane structures from NMR as before, yields 38.94% Si, in perfect agreement with the measured value. Apparently, the amount of

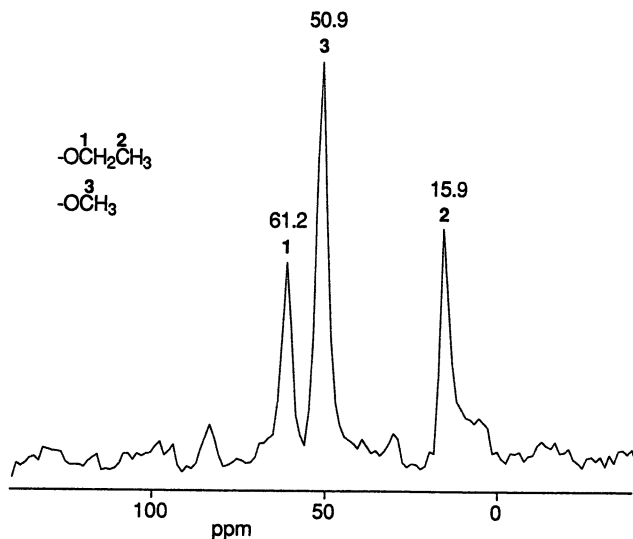


Figure 4.—Continued. Part c: M1, 3000 accumulations.

Table IV. Elemental Analysis (Weight Percentages)

System	C (%)	H (%)	N (%)
A1 <sup>a</sup>	1.68 ± 0.01 <sup>b</sup>	0.97 ± 0.08	
A1	1.11 ± 0.02	0.99 ± 0.08	
A1APS	7.29 ± 0.01	2.20 ± 0.03	2.18 ± 0.02
A2	0.59 ± 0.01	0.85 ± 0.02	
A3S	9.7	2.7	
A5 <sup>a</sup>	5.07 ± 0.12	1.66 ± 0.07	
A5APS	6.03 ± 0.05	2.05 ± 0.04	0.32 ± 0.01
A6	3.95 ± 0.04	1.55 ± 0.08	
A6 <sup>c</sup>	3.54 ± 0.03	1.45 ± 0.08	
Mix1	12.95 ± 0.02	3.97 ± 0.07	4.49 ± 0.05
P1	3.84 ± 0.02	1.55 ± 0.04	
P1 <sup>c</sup>	0.27 ± 0.04	1.34 ± 0.10	
Compol	0.1 ± 0.01	0.23 ± 0.02	

<sup>a</sup>Samples underwent the coating conditions.

<sup>b</sup>Errors indicate differences in duplicate results.

<sup>c</sup>Samples were washed for 3 h with water before drying.

physically absorbed water can be neglected in this case. This is not so strange, considering the heating to 190 °C for 3 h during esterification. Jansen, et al. (8) stated that 5% H<sub>2</sub>O was present inside the particles, but this error was made because it was assumed that only Q<sup>4</sup> was present.

Figure 5 shows all the possible silicon signals that can be obtained from reactions between TES and APS. Carbon assignments will be described in more detail elsewhere (50). The chemical shifts compare well

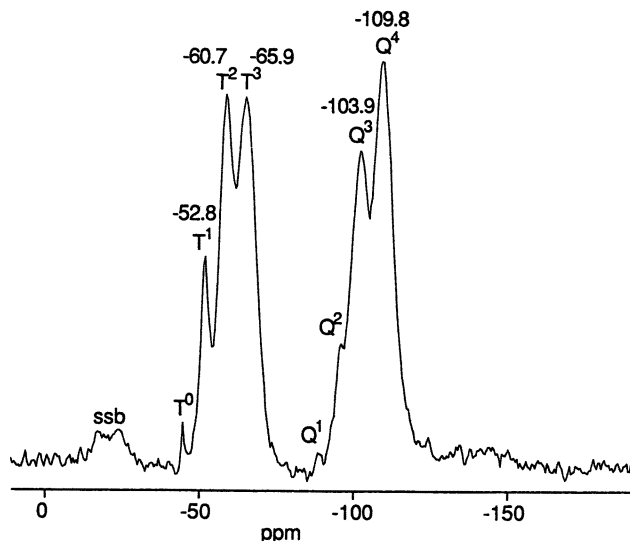


Figure 5.  $^{29}\text{Si}$  CP-MAS NMR spectra of a mixture of TES-APS hydrolyzed by atmospheric water; 2000 accumulations and contact time of 4 ms.

with literature data (36–40, 54–56). This test sample was made by mixing equal amounts of TES and APS and letting the mixture hydrolyze by atmospheric water. The white powder thus obtained (no colloidal spheres) was crushed and placed in a spinner. The quantitative silicon spectra obtained from A1APS and Mix1 did not contain signals from T<sup>1</sup>, but were similar.

For the APS-coated A1APS, the silicon nuclei of APS could be determined quantitatively with NMR spectroscopy (Table III). For 1 g of A1APS, as explained before, one calculates 1.68 mmol of APS. Using the N percentages gives 1.56 mmol of APS. The difference, 0.12 mmol, can be explained by assuming that a few percent physically adsorbed water was also present. The number of Q<sup>3</sup> and Q<sup>2</sup> becoming Q<sup>4</sup> because of the coating reaction is clearly lower than the number of T species formed (Table III). This result shows that APS did not form all its siloxane bonds with Q species.

Unfortunately, the coating of A5 contained too few APS to be determined with NMR spectroscopy. Comparing the surface-to-volume ratio of A1 and A5 using the TEM radius gives a value of 6.9; the ratio of the N percentages is 6.8. Probably, the amount of coating scales with the surface available and the reaction stops if the silanols belonging to Q species are not available anymore. For A5 this means that only 1.1% of the available APS actually ended up on the particle surface. Without the silica particles, the APS does not form any structure that scatters light (50).

These surface coverages are somewhat less than the coating with methacryloxypropyltrimethoxysilane as described by Philipse and Vrij (4). He calculates  $\sim 10$  groups per square nanometer. Using the values of A5 one finds  $\sim 2$  APS molecules per square nanometer. Badley, et al. (11) found for particles of radius 58.1 nm with elemental analysis 0.90% N. The difference with this work was that the concentration of APS was approximately 10 times smaller and no refluxing or distillation was used, but the reaction was continued for 20 h. The methoxy derivative of APS also was used, probably resulting in faster hydrolysis. Apparently, APS reacts very slowly with silica.

The results obtained for Mix1 are amazing: 36.3% of the APS used ended up inside the particles (Table IV). This value contrasts sharply with the small amount found in the coating reaction, even though the concentrations used there were higher. The APS did not end up as a surface coating, as is indicated by the very low amount of Q<sup>4</sup>. This result can only be explained if the APS is distributed through a large portion of the colloid.

As before, calculating the amount of APS per gram using SiO<sub>x</sub> gives 3.28 mmol and, from the percent N one gets 3.19 mmol. The small difference is again probably due to a few percent H<sub>2</sub>O. The amount of carbon also indicates that 5% of the Si atoms can still be bonded to an ethoxy group.

**Nucleation and Growth Mechanism.** In the following sections, we will test some of our findings with predictions and assumptions of the proposed mechanisms in the literature.

The finding that a few percent of ethoxy groups never leave the TES molecule is in accordance with the findings of Harris and co-workers (16, 18) and Matsoukas and Gulari (17, 22) that the growth rate of the silica particles is limited by the hydrolysis of TES. Under these conditions, some monomers may polymerize before the hydrolysis of all the groups on the silicon atom is complete. Were the hydrolysis complete in the first few minutes, it would indeed seem strange to find ethoxy groups in the methanosol and propanosol. This kind of reasoning can also be used to explain the large amount of APS that was build inside the Mix1 Particles. Here, hydrolyzed TES molecules could have reacted with the slower hydrolyzing APS molecules.

We find a contradiction with the assumptions made by Bogush and co-workers (24–27) that in the first few minutes all TES hydrolyzes and that during the whole particle growth the nucleation continues. If growth continued through aggregation of subparticles during the whole process, the surfaces of the spheres that can be seen in Figure 2c and 2g could not have been as smooth.



In our work and from the literature (1, 2, 24–27), it can be seen that particles with a radius of 15 nm to about 400 nm can be made with a single concentration of TES by changing only the amount of ammonia. This is a 25-fold increase in radius. Using equations 3 and 4 derived by Matsoukas and Gulari in their kinetic model yields for the ratio of hydrolysis and polymerization rate constants  $2.4 \times 10^8$  and  $3.8 \times 10^{12}$  for the diffusion and reaction-limited cases, respectively. Both the hydrolysis and polymerization are caused by a nucleophilic reaction mechanism; hence, such an increase of one over the other is very unlikely. The factor  $2.4 \times 10^8$  is also very far from the differences in reaction rates that have been determined experimentally by Harris and co-workers (16, 18). Therefore, although the model of Matsoukas and Gulari (22) seems to explain the polydispersity and growth of a particle distribution, it fails to predict the final size. This deficiency is because their kinetic model is also used to describe the particle nucleation process.

However, if we use the expressions for the classical nucleation rate, we also do not find the large increase in radius that is possible. Furthermore, Weres et al. (57) state that addition of NaCl to a homogeneous nucleating solution of silicic acid in water has only a moderate effect if the concentrations are below 1 M. Addition of salt to the reaction mixture of the Stöber process has, however, very large effects. Clearly, classical nucleation cannot explain all the features of the Stöber synthesis either.

One possible solution is to assume that the number of nuclei that have been formed through homogeneous nucleation decreases early in the reaction by a controlled aggregation process. After, and perhaps during, the short aggregation period, monodispersity is reached by the addition of monomers or small oligomers. The assumption that small silica particles are not stable against aggregation can be made plausible as follows: The silica particles in an alcosol derive their stability from the negative surface charge originating from dissociated silanol groups. Preliminary conductivity and electrophoretic measurements on the A6 particles in the reaction mixture indicate a surface potential of about 50 mV, a low, reasonable value. This value has also been reported by Bogush et al. (24) but it is very difficult to make an accurate interpretation of the measurements. Many of the important physical properties of the alcosol mixture are not exactly known. A better indication of the stability of the particles comes from the observation of the flocculation concentration of 5 mM LiNO<sub>3</sub>. At a concentration of 1 mM, the sol remains stable, but the final particle radius is almost doubled (A6–A8, Tables I, II) *only* if the salt is added before the first particles are visible! When a concentration of 2 mM was added, the sol flocculated during its formation.

The Derjaguin–Landau–Verwey–Overbeek (DLVO) theory of charged colloids (58) predicts a substantial decrease in stability against flocculation with decreasing particle radius. Most likely the newly formed

nuclei are not yet stabilized, and stability sets in only after a certain radius is obtained. After this size is reached, particles grow through monomer addition either reaction- or diffusion-limited, but with an overall rate still depending on the hydrolysis.

The finding that particles increase in size by using more ammonia (Table I), in spite of the fact that this increases the surface charge, probably involves an increase in ionic strength that compresses the double layer. As reported by Bogush (27), during the first minutes of the reaction, there is a sharp increase in solution conductivity that decreases slowly during the remainder of the reaction. The production of silicic acid, partly dissociated by  $\text{NH}_3$ , causes this increase. When the particles grow, the number of available silanol groups slowly decreases, and so does the conductivity. This sudden increase in ionic strength is probably higher for higher concentrations of ammonia and results in larger particles. Clearly, these predictions have to be verified experimentally (49).

Eventually, the effect on the surface charge of the increase in  $[\text{NH}_3]$  and  $[\text{H}_2\text{O}]$  overcomes the increase in ionic strength, and the decrease in the number of nuclei is less, so that the particle radius decreases.

The model as proposed can also explain why solvents with a higher dielectric constant produce smaller particles and why, under conditions where the largest particles are formed, the sols sometimes flocculate.

Finally, the particle morphology must be explained in terms of the nucleation or growth mechanism. We tentatively assume that the irregular shape of some particles (for instance, A3 and A1) is caused by the proposed controlled aggregation mechanism early in the formation of the particles. For these systems the monomer growth was not yet able to create a smooth surface, as present on the larger spheres like A6. A2 also has very spherical and smooth particles, but here the low TES and high water concentration stabilized the aggregating particles at a small radius before most of the TES was used and a smooth particle surface could be achieved.

## Conclusions

We conclude that hydrolysis is the rate-limiting step in growth because a few percent of the ethoxy groups of TES are not hydrolyzed fully before they polymerize and these groups are also included in the interior of the larger particles. This conclusion can also be drawn from more direct measurements presented in the literature (16–18, 22).

We propose that silica particles synthesized according to the method of Stöber are formed through a controlled aggregation of nuclei formed through homogeneous nucleation, followed by growth through monomer addition. The ionic strength is an important parameter in the determination of the final particle size, and it is easily changed by addition of salt (49).

Silica particles can be coated by the silane coupling agent APS in the reaction medium to obtain stable colloids. These systems can be used to further bind relevant groups to the particle surface (48, 51, 52). Quantitative  $^{29}\text{Si}$  NMR spectroscopy appears to be a valuable tool in characterizing a new kind of stable colloidal particles synthesized from a mixture of the alkoxides APS and TES. These monodisperse, spherical particles can already be prepared with a low polydispersity and contain APS molecules distributed through an important part of the bulk of the particle. It would be interesting to see whether this method is also applicable to other mixtures of alkoxides. More work concerning the characterization of these new systems has to be done (50).

### Acknowledgments

We thank G. Nachtegaal and Dr. A.P.M. Kentgens for their help with the NMR measurements at the SON-NWO HF-NMR facility (Nijmegen, the Netherlands). We also thank J. Suurmond and J. Pieters for performing the electron microscopy, and A. Philipse for his comments.

This work was supported by the Netherlands Foundation for Chemical Research (SON) with financial aid from the Netherlands Organization for Scientific Research (NWO).

### References

1. Stöber, W.; Fink, A.; Bohn, E. *J. Colloid Interface Sci.* **1968**, *26*(1), 62–69.
2. Van Helden, A. K.; Jansen, J. W.; Vrij, A. *Colloid Interface Sci.* **1981**, *81*(2), 354–368.
3. Van Helden, A.K.; Vrij, A.J. *Colloid Interface Sci.* **1980**, *78*(2), 312–329.
4. Philipse, A. P.; Vrij, A. *J. Colloid Interface Sci.* **1989**, *128*(1), 121–136.
5. Philipse, A. P. *Colloid Polym. Sci.* **1988**, *266*(12), 1174–1180.
6. Philipse, A. P.; Smits, C.; Vrij, A. *J. Colloid Interface Sci.* **1989**, *129*(2), 335–352.
7. Philipse, A. P.; Vrij, A. *J. Chem. Phys.* **1987**, *87*(10), 5634–5643.
8. Jansen, J. W.; De Kruif, C. G.; Vrij, A. *J. Colloid Interface Sci.* **1986**, *114*(2), 481–491.
9. Moonen, J.; Pathmanathan, C.; Vrij, A. *J. Colloid Interface Sci.* **1989**, *131*(2), 349–365.
10. Plueddemann, E. P. *Silane Coupling Agents*; Plenum: New York, 1982.
11. Badley, R. D.; Ford, W. T.; McEnroe, F. J.; Assink, R. A. *Langmuir* **1990**, *6*, 792–801.
12. Noll, W. *Chemie und Technologie der Silicone*; 2nd ed.; Verlag Chemie GmbH: Weinheim, Germany 1968.
13. Aelion, B. R.; Loebel, A.; Eirich, F. *J. Am. Chem. Soc.* **1950**, *72*, 5705–5712.
14. Keefer K. D. *Mater. Res. Soc. Symp. Proc.* **1984**, *32*, 15–24.
15. Brinker, C. J.; Scherer, G. W. *Sol-Gel Science*; 1st ed.; Academic Press: Boston, MA, 1990.
16. Byers, C. H.; Harris, M. T.; Williams, D. F. *Ind. Eng. Chem. Res.* **1987**, *26*(9), 1916–1923.

17. Matsoukas, T.; Gulari, E. *J. Colloid Interface Sci.* **1988**, *124*(1), 252–261.
18. Harris, M. T.; Brunson, R. R.; Byers, C. H. *J. Non-Cryst. Solids* **1990**, *121*, 307–403.
19. Schaefer, D. W.; Keefer, K. D. *Phys. Rev. Lett.* **1984**, *53*(14), 1383–1386.
20. Iler, R. K. *The Chemistry of Silica*; Wiley & Sons: New York, 1979.
21. Plueddemann, E. P. In *Silylated Surfaces*; Leyden, D. E.; Collins, W. T., Eds.; Gordon & Breach: New York, 1980; pp 31–53.
22. Matsoukas, T.; Gulari, E. *J. Colloid Interface Sci.* **1989**, *132*(1), 13–21.
23. Coenen, S.; De Kruif, C. G. *J. Colloid Interface Sci.* **1988**, *124*(1), 104–110.
24. Bogush, G.; Zukoski, C. *The Colloid Chemistry of Graving Silica Spheres*; Ceramic Microstructures 1986; Plenum Press: New York, 1987; pp 475–483.
25. Brinker, C. J.; Scherer, G. W. *Sol-Gel Science*; 1st ed.; Academic Press: Boston, MA, 1990; pp 199–203.
26. Bogush, G. H.; Tracy, M. A.; Zukoski, C. F., IV *J. Non-Cryst. Solids* **1988**, *104*, 95–106.
27. Bogush, G. H.; Dickstein, G. L.; Lee, P.; Zukoski, C. F., IV *Mater. Res. Soc. Symp. Proc.* **1988**, *121*, 57.
28. Adams, J.; Baird, T.; Braterman, P. S.; Cairns, J. A.; Segal, D. L. *Mater. Res. Soc. Symp. Proc.* **1988**, *121*, 361–371.
29. Makrides, A. C.; Turner, M.; Slaughter, J. *J. Colloid Interface Sci.* **1973**, *73*(2), 345–367.
30. Nielsen, A. E. *Kinetics of Precipitation*; Pergamon Press: Oxford, England, 1964.
31. Feeney, P. J.; Napper, D. H.; Gilbert, R. G. *Macromolecules* **1984**, *17*, 2520–2529.
32. La Mer, V. K.; Dinegar, R. H. *J. Am. Chem. Soc.* **1950**, *72*, 4847.
33. Overbeek, J. Th. G. *Adv. Colloid Interface Sci.* **1982**, *15*, 251–277.
34. Keefer, K. D. In *A Model for the Growth of Fractal Silica Polymers*; Hench, L. L.; Ulrich, D. R., Eds.; Science of Ceramic Chemical Processing; Wiley & Sons: New York, 1986; pp 131–139.
35. Schaefer, D. W.; Keefer, K. D. *Mater. Res. Soc. Symp. Proc.* **1986**, *72*, 277–287.
36. Sindorf, D. W.; Maciel, G. E. *J. Am. Chem. Soc.* **1981**, *103*, 4263–4265.
37. Sindorf, D. W.; Maciel, G. E. *J. Am. Chem. Soc.* **1983**, *105*(12), 3767–3776.
38. Sindorf, D. W.; Maciel, G. E. *J. Phys. Chem.* **1982**, *86*(26), 5208–5219.
39. Fyfe, C. A.; Gobbi, G. C.; Kennedy, G. J. *J. Phys. Chem.* **1985**, *89*(2), 277–281.
40. Fyfe, C. A. *Solid State NMR for Chemists*; CFC Press: Ontario, Canada, 1983.
41. Penders, M. H. G. M.; Vrij, A. *Colloid Polym Sci.* **1991**, *286*, 823–831.
42. Duits, M. H. G.; May, R. P.; Vrij, A.; De Kruif, C. G. *J. Chem. Phys.* **1991**, *94*, 4521–4531.
43. Koppel, D. E. *J. Chem. Phys.* **1972**, *57*(11), 4814.
44. *Dynamic Light Scattering: Applications of Photon Correlation Spectroscopy*; Pecora, R., Ed.; Plenum: New York, 1985.
45. Kops-Werkhoven, M. M.; Fijnaut, H. M. *J. Chem. Phys.* **1981**, *74*(3), 1618–1625.
46. Van Veluwen, A.; Lekkerkerker, H. N. W.; De Kruif, C. G.; Vrij, A. *J. Chem. Phys.* **1988**, *89*(5), 2810–2815.
47. Van Blaaderen, A.; Van Geest, J.; Vrij, A. *J. Colloid Interface Sci.* **1992**, *154*(2), 481–501.
48. Van Blaaderen, A.; Vrij, A. *Langmuir* **1992**, *8*, 2921–2931.
49. Van Blaaderen, A.; Kentgens, A. P. M. *J. Non-Cryst. Solids* **1992**, *149*, 161–178.

50. Van Blaaderen, A. Vrij, A. *J. Colloid Interface Sci.* **1993**, *156*, 1–18.
51. Van Blaaderen, A.; Peetermans, J.; Maret, G.; Dhont, J. K. G. *J. Chem. Phys.* **1992**, *96*(6), 4591–4603.
52. Van Blaaderen, A. *Adv. Mater.* **1993**, *5*(1), 52–54.
53. De Rooy, N. Ph.D. Dissertation, University of Utrecht, Utrecht, Netherlands, 1979.
54. Chiang, C. H.; Liu, N. I.; Koenig, J. L. *J. Colloid Interface Sci.* **1982**, *86*(1), 26–34.
55. Vankan, J. M. J.; Ponjee, J. J.; De Haan, J. W.; Van de Ven, L. J. M. *J. Colloid Interface Sci.* **1988**, *126*(2), 604–609.
56. De Haan, J. W.; Van den Bogaert, H. M.; Ponjee, J. J.; Van de Ven, L. J. M. *J. Colloid Interface Sci.* **1986**, *110*(2), 591–600.
57. Weres, O.; Yee, A.; Tsao, L. *J. Colloid Interface Sci.* **1980**, *84*(2), 379–402.
58. Verwey, E. J. W.; Overbeek, J. Th. G. *Theory of the Stability of Lyophobic Colloids*; Elsevier: New York, 1948.

RECEIVED for review December 17, 1990. ACCEPTED revised manuscript March 30, 1992.